Spectral Evaluation of Laser-Induced Cell Damage With Photothermal Microscopy

Dmitri O. Lapotko, PhD[1] and Vladimir P. Zharov, PhD[2]*
[1]*Luikov Heat and Mass Transfer Institute, International Research Centre, Minsk, Belarus*
[2]*Philips Classic Laser Laboratories, University of Arkansas for Medical Sciences, Little Rock, Arkansas*

Background and Objectives: Determining cell photodamage is important for laser medicine and laser safety standards. This work evaluated the potential of photothermal (PT) technique for studying invasive laser-cell interaction, with a focus on PT evaluation of spectral dependence of laser-induced damage in visible region at single intact cell level.
Study Design/Materials and Methods: PT is based on irradiation of a single intact cells with a tunable pump laser pulse (420–570 nm, 8 nanoseconds, 0.1–300 μJ) and monitoring of temperature-dependent variations of the refractive index with a second, collinear probe beam in pulse (imaging) mode (639 nm, 13 nanoseconds, 10 nJ), and continuous (integrated PT response) mode (633 nm, 2 mW). The local and the integrated PT responses from the individual living red blood cells, lymphocytes, and cancer cells (K562) in vitro were obtained at different pump laser fluence and wavelength and compared with data obtained by conventional viability tests (Annexin V—propidium iodide).
Results: The cell damage with pump pulse lead to specific change in PT response's temporal shape and PT image's structure. The photodamage thresholds varied in the range of 0.5–5 J/cm^2 for red blood cells, 4.4–42 J/cm^2 for lymphocytes, and 36–90 J/cm^2 for blast cells in the pump wavelength range of 417–555 nm.
Conclusion: Damage threshold at different wavelength depends on absorption spectra of cells. Spectral evaluation of laser-damage thresholds can be done in two supplements for each PT mode—PT imaging and integrated PT response. The correlation between specific change of PT parameters and cell damage permits using PT technique to rapidly estimate the invasive conditions of the laser-cell interactions. Lasers Surg. Med. 36:22–30, 2005.

Key words: laser; cell; photodamage; photothermal effects; spectroscopy; viability tests

INTRODUCTION

Short-term laser-induced local tissue overheating may have various effects at the cellular level, such as changes in cell metabolism, molecular photoconformation, protein denaturation, acoustic wave formation, bubble formation, and photomechanical stress. As a result, such local overheating leads to loss of cell viability and cell damage [1–22]. Most research in this area has focused on tissue-level effects; only a few studies have examined cell-level effects, and those have mainly focused on cells containing relatively strong-absorbing chromophores, such as red blood cells (RBCs) with hemoglobin or retinal pigmented cells (melanosomes with melanin) [8–10,16,17,21,22]. Researchers have observed that laser-induced bubble formation around such strongly absorbing zones causes cell damage. However, the thresholds and mechanisms of photodamage for many others, less absorbent cells in the visible-light spectral range (e.g., white blood cells, various cancer cells) are still not clear [23]. This lack of knowledge may result from the inability of conventional methods (e.g., time-resolved transmission, reflectance, and other types of microscopy) to measure short-term local thermal phenomena and their consequences in single living intact cells with sufficient sensitivity and resolution in a broad spectral range.

Recently, the photothermal (PT) technique has shown the capability to visualize photo-damage related phenomena at one laser wavelength [24]. We have extended here this technique to study spectral dependence of photodamage threshold of red blood cells, lymphocytes, and tumor cells (K562) at single cell level. Specifically, our purpose was investigating dependence of the conditions of individual cell damage upon laser- and cell-related factors: laser pulse fluence and wavelength, heterogeneity of cell properties in cell population. Our other purpose was evaluating the sensitivity and selectivity of PT method in monitoring laser-induced damage in tissue at cell level. For that, we have chosen three types of cells:

- Red blood cells (RBC) with spatially uniform light absorption by hemoglobin inside those cells;
- Lymphocytes and tumor cells with spatially heterogeneous light absorption.

*Correspondence to: Vladimir P. Zharov, PhD, Philips Classic Laser Laboratories, University of Arkansas for Medical Sciences, 4301 West Markham St., Slot 543, Little Rock, Arkansas 72205-7199. E-mail: ZharovVladimirP@uams.edu
V.P.Z. has disclosed a potential financial conflict of interest with this study.
Accepted 27 October 2004
Published online in Wiley InterScience (www.interscience.wiley.com).
DOI 10.1002/lsm.20119

MATERIALS AND METHODS

PT Technique

The general principles of the PT technique have already been reported [24–29]. Thermal-lens (thermolens) mode permitted the recording of a whole-cell's time-resolved integrated PT response via focusing/defocusing effects (depending on the polarity of refractive index changes and the optical scheme) of a collinear, intensity-stabilized, continuous-wave helium–neon (He–Ne) probe laser beam (wavelength, 633 nm; diameter, 15 μm; energy, 1.4 mW; model 117A, Spectra-Physics, Inc.) detected by a photodiode (C5658; Hamamatsu Corp.) (Fig. 1). The PT cell response was recorded with a Tektronix TDS 3032B oscilloscope, as well as a digital PC board (Bordo-210; Diagnostic Systems, Minsk, Belarus), and was analyzed with customized software. PT responses were classified according to their types. Type 1 is standard response that is caused by heating–cooling process without cell damage. Its shape features sharp front and gradual tail and this response has positive polarity. Type 2 response has a peak of negative polarity of nearly symmetrical shape and this response was shown to be associated with cell damage [25,26].

In addition to this mode, in a second-PT imaging (PTI) mode the single cell was irradiated with a short, focused pump laser pulse (tunable optical parametric oscillator; wavelength, 420–570 nm; pulse width, 8 nanoseconds; pulse energy, 0.1–400 μJ; Lotis Ltd., Minsk, Belarus). Time-resolved monitoring of temperature-dependent variations of the refractive index in the cell was accomplished with phase-contrast imaging (Olympus BX51 microscope with a CCD camera, AE-260E, Apogee, Inc.) using a second, collinear laser pulse (Raman shifter; wavelength, 639 nm; pulse width, 13 nanoseconds; pulse energy, 10 nJ) with a tunable time delay between pump and probe pulses (0–5,000 nanoseconds) (Fig. 1). After passing through the sample, pump radiation was cut off with a filter. A special phase micro-objective with a moderate numerical aperture (20×, N.A. 0.4) and Zernike coaxial quarter-wave spots with a transmission of 30% and a diameter of 0.7 mm (more suitable for laser experiments) were used to provide phase-contrast imaging of the probe laser beam.

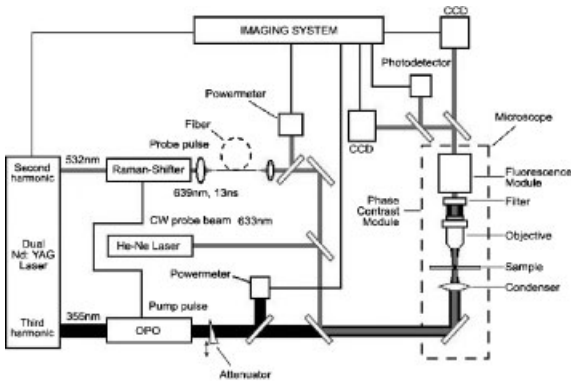

Fig. 1. Experimental setup: Laser PT phase-contrast microscope/spectrometer.

The diameters of pump- and probe-beam spots were 23 μm and 17 μm, respectively. As a result, formation of a PT image required just one pump pulse with a relatively broad beam diameter covering entire single cells with typical sizes in the range of 6–12 μm. Time-consuming scanning with a strongly focused laser beam across each individual cell, as in conventional laser imaging, was unnecessary. With this arrangement, a spatial resolution of approximately 0.7 μm was determined by microscope objective aperture rather than by laser-beam diameter. The entire PT-image-acquisition procedure included illumination of the cell with three pulses: an initial probe pulse followed by a 0.1-second delay to the pump pulse, and then a second probe pulse with a tunable delay (0–5,000 nanoseconds) to the pump pulse. The PT image was calculated as the difference between the two probe images [28] and depended only on absorption contrast transformed by the pump laser pulse into refractive contrast, rather than on possible phase distortion of the probe beam itself, natural refractive intracellular heterogeneities, and especially, scattered light. The chosen energy of the probe laser pulse (~10 nJ) was much lower than the pump-pulse energy permitted, thus minimizing the influence of probe-beam absorption by objects. The pump and probes beams had a stable, Gaussian intensity profile (controlled with the CCD camera), and the diameter of the laser beams was larger than that of the cells themselves (see above). Consequently, the possible influence of a non-smooth intensity distribution in cross-section (including hot spots) on cells was practically negligible (see below). Simultaneously with the capture of images, probe- and pump-pulse energy levels were measured with photodiodes (Fig. 1), and the amplitude of each image pixel was normalized on laser pulse energy, which permitted the necessary compensation for possible variations in laser energy from pulse to pulse. The measurement of PT images at different time delays between pump and second probe beam in pulse-repetition mode allowed time-resolved monitoring of the temporal dynamic of local PT amplitudes from different absorbing zones in each cell. PT images can be also used to detect cell damage by laser pulse: in case of the damage PT image will indicate specific positive peaks.

Evaluation of Cell Damage With PT Method

According to laser load test (LLT) [24,26] cell was considered to be damaged if the following conditions applied: (1) a difference between the two PT signals was detected after the first and second laser pulses, (2) the type of PT response changed from type 1 to type 2 (type 1 is linear "positive" PT responses and type 2 is non-linear PT responses with "negative" component—see below), and (3) an independent conventional viability test performed in parallel with the PT assay confirmed damage. To estimate non-linear effects caused by cell damage with the PT method, we measured the level of cells in popiulation in which irradition with a laser pulse produced PT signals with a negative component only. The two quantitive parameters were used:

(a) Probability of cell damage (PR2). That is obtained as the percentage of cells with PT signals with a negative component and is calculated as $PR2 = N_{neg}/N$, where N is the total number of cells irradiated with just one laser pulse and N_{neg} is the number of cells with a PT signal with a negative component. In all, 100 cells were studied, and all experiments were performed three times under the same conditions.
(b) Laser fluence that is defined as photo-damage threshold and is obtained from experimental curve PR2(E). In general, the dose required to reach the damage threshold (fluence energy dose [ED_{50}]) was defined as a laser energy fluence rate that induced the damage in 50% of the cell population.

Measuring energy's and PT-response's stability. Pulse-to-pulse energy during 20 pulses (i.e., pump-pulse energy stability, which is important in the study of many cells) was measured with an Ophir PE10/Nova-calibrated energy meter (Ophir Optronics, Inc., Danvers, MA). Energy stability was in the range of 2.8%–3.8% (560 nm and 420 nm, respectively) for the whole beam and was approximately 6.5% for local points of the beam (i.e., hot spots).

Cell Preparation

Living cells studied with the PT technique included RBCs, peripheral blood lymphocytes, and a human leukemia cell line (K562). Cells were studied in suspension in vitro. All cells were prepared according to established procedures at the University of Arkansas for Medical Sciences. In particular, K562 cells were grown in a 25-cm^3 tissue culture flask in RPMI 1640 solution (Sigma-Aldrich) with 10% fetal calf serum, glutamine, and penicillin/streptomycin. K562 cells were cultured at 37°C in 7% carbon dioxide. Before use, the cells were washed twice with phosphate-buffered saline (PBS) and resuspended at 3×10^6 cells/ml in serum-free RPMI 1641 without phenol red.

Lymphocytes were prepared by in PBS and subjected to centrifugation over Ficoll-Paque (Amersham Biosciences) to separate lymphocytes from RBCs, granulocytes, and platelets. Lymphocytes were washed twice in PBS and resuspended at 3×10^6 cells/ml in serum-free RPMI 1641 without phenol red. For the preparation of RBCs, blood mixed with disodium ethylenediaminetetraacetic acid (EDTA) was diluted with a 0.15M sodium chloride solution to reach a cell concentration of 1×10^8 cells/ml.

A comparison of PT data obtained with cells in suspension on conventional slides, cells fixed on substrate, and cells in suspension in a slide with 0.12-mm gasket glasses has demonstrated advantages for the latter system, which has been used in many experiments at room temperature. Each cell was chosen on the basis of its optical image and positioned with the microscope stage in the center of the laser beams. To avoid pump-pulse cumulative effects, measurements were taken by irradiating one cell with a single pulse at a specific energy level and then irradiating another cell from the same population at the same energy level, and so on. The procedure was then repeated at other energy levels with other cells.

Cell Viability Testing

Cell viability was determined before and after the PT experiments by staining the cells with the use of trypan blue dye or Annexin V—propidium iodide (PI) kits (Roche Diagnostics Corp.), after which fluorescence imaging was performed and cells penetrated by the dye were counted. The approach made it difficult to obtain reliable statistical data during the independent conventional cell viability test because one-by-one irradiation of many cells with focused beam in PT microscope was time-consuming. To overcome this problem, we used a broader laser beam, which was obtained by splitting the more powerful second harmonic beam from the pump laser (532 nm) before the firing of the second, collinear Raman shifter pulse (Fig. 1). We also used a more powerful second laser (a continuous-wave biomedical Medlite IV) with parameters similar to those of the pump laser in the PT microscope (wavelength, 532 nm; pulse width, 12 nanoseconds). The broad beams of both lasers, which had a Gaussian intensity profile and the same diameter (2.5 mm at level e), were used to irradiate cells in suspension in a quartz cuvette with a 2×10-mm cavity. Use of a 2-mm diameter pinhole in front of the cuvette provided a smooth beam-intensity profile into the cuvette. This setup allowed simultaneous irradiation of 100,000–500,000 cells at a cell concentration of 10^6–10^7 ml^{-1} in a 50-μl suspension volume. Comparison data obtained with both lasers despite a slight difference in their pulse duration (8 and 12 nanoseconds) did not reveal notable differences in cell damage, so further experiments were performed with a second laser.

RESULTS

Stability and Reproducibility

Preliminary measurements of the stability of the integrated PT responses and the PT images from pulse to pulse (3-second intervals between each pulse) for single cells at different laser energy levels showed good stability at low pulse-energy levels (see the levels in Figs. 3 and 4). At higher energy levels, however, many cells demonstrated some degradation of the PT response, except for RBCs, which were more stable. For example, after ten pulses at a 427-nm wavelength, decreases in PT-response amplitude were as follows: for lymphocytes at 50 μJ and 100 μJ, 15% and 3.5 times, respectively; for K562 cells at 50 μJ and 250 μJ, 25% and one order of magnitude, respectively. This effect was found to be energy-dependent and, at higher energy levels, could occur after just a few pump pulses or even just one. For this reason, in further experiments, most PT-response measurements as a function of laser energy level were performed with only a single pump laser pulse. In LLT mode we have determined minimal amount of cells that are required to obtain statistically reproducible data. For that purpose we have measured parameter PR2 as function of number of studied K562 cells (Fig. 2). Most heterogeneous cells among all studied by us were used for this experiment and as can be seen from Fig. 2 even 50 cells is sufficient to measure the value PR2.

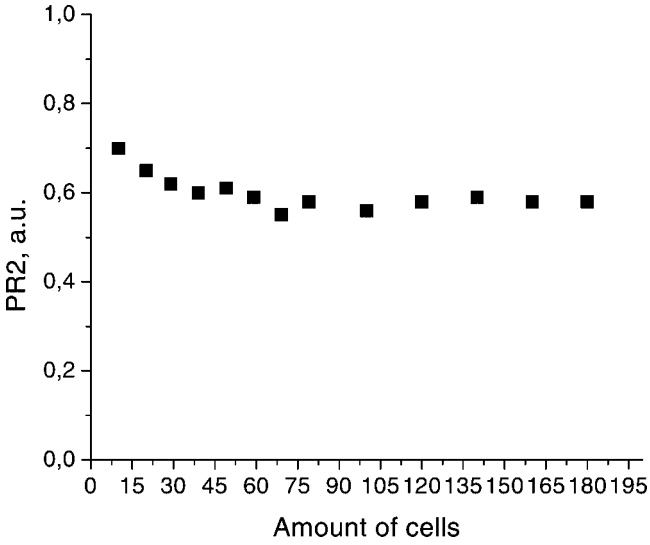

Fig. 2. Dependence of cell damage probability PR2 (K562 cells) upon the number of irradiated cells at fixed laser fluence.

PT Images of Individual Cells

Figure 3 shows PT images of different cells obtained at three energy levels (one less than and the others greater than the damage threshold) compared with conventional optical images. Non-invasiveness for a specific pump energy level was verified by cell viability testing after the cell population was irradiated with a single pump pulse. The pump pulse was viewed as producing no cellular photodamage if $\geq$94% of the cells were viable after exposure to the pulse. Under non-invasive conditions, PTI mode visualized local heat release, which might correspond to the spatial distribution of absorbing cellular structures (Fig. 3, second column) [24,28] that were invisible with the much less sensitive conventional transmission microscopy (Fig. 3, first column). At a higher energy level constituting an invasive condition, PTI visualized high amplitude peaks that were found to appear in cells that later have uptaken trepan blue and therefore were damaged. Thus such peaks in PT images were considered in similar way as type-2 responses and were treated as indicators of cell damage.

PT Responses From Individual Cells

PT responses (signals) were obtained for the same cells under the same conditions as used for study PT images. The amplitude of the PT signal increased with increases in the pulse energy level until local temperature reached saturation thresholds. It should be noted that at low energy levels, we measured a positive peak PT amplitude; however, at higher energy levels, PT response was saturated and hidden by a large negative peak. As a result, the integral PT-response amplitude decreased at higher energy

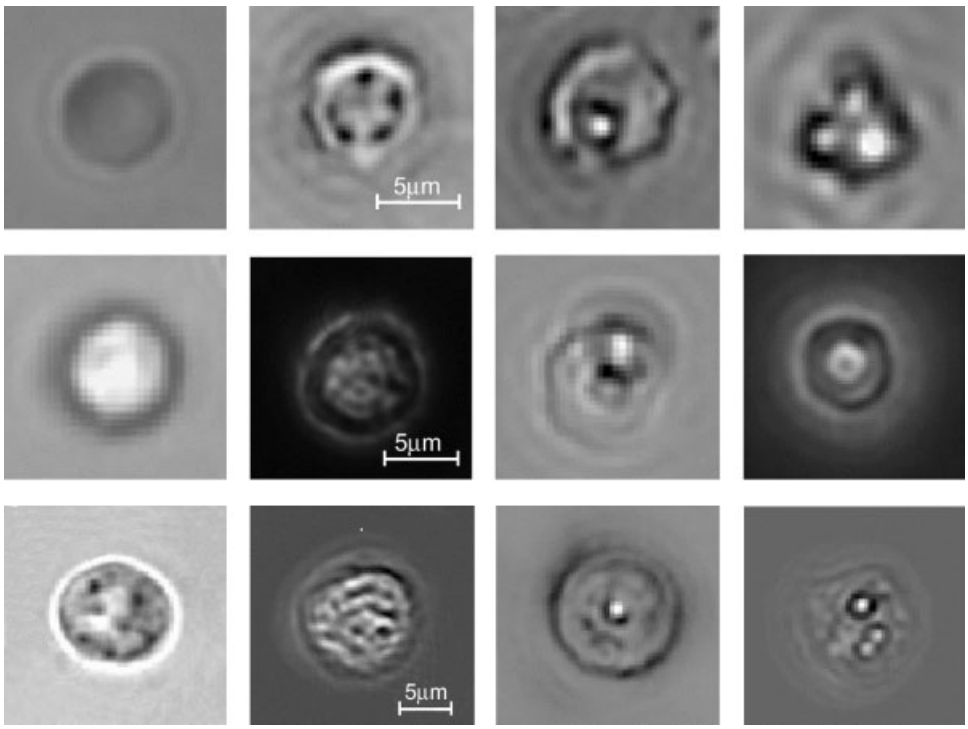

Fig. 3. Conventional transmission (first column) and PT images of different cells at different laser energy levels below (second column) and above (third and fourth columns) the damage threshold. Cells/wavelength/time delay/energy levels (from second column, left to right): First row, RBCs/532 nm/30 nanoseconds/1.4 μJ, 3 μJ, and 8 μJ; second row, lymphocytes/427 nm/100 nanoseconds/30 μJ, 150 μJ, and 250 μJ; third row, K562 cells/427 nm/10 nanoseconds/50 μJ, 100 μJ, and 150 μJ.

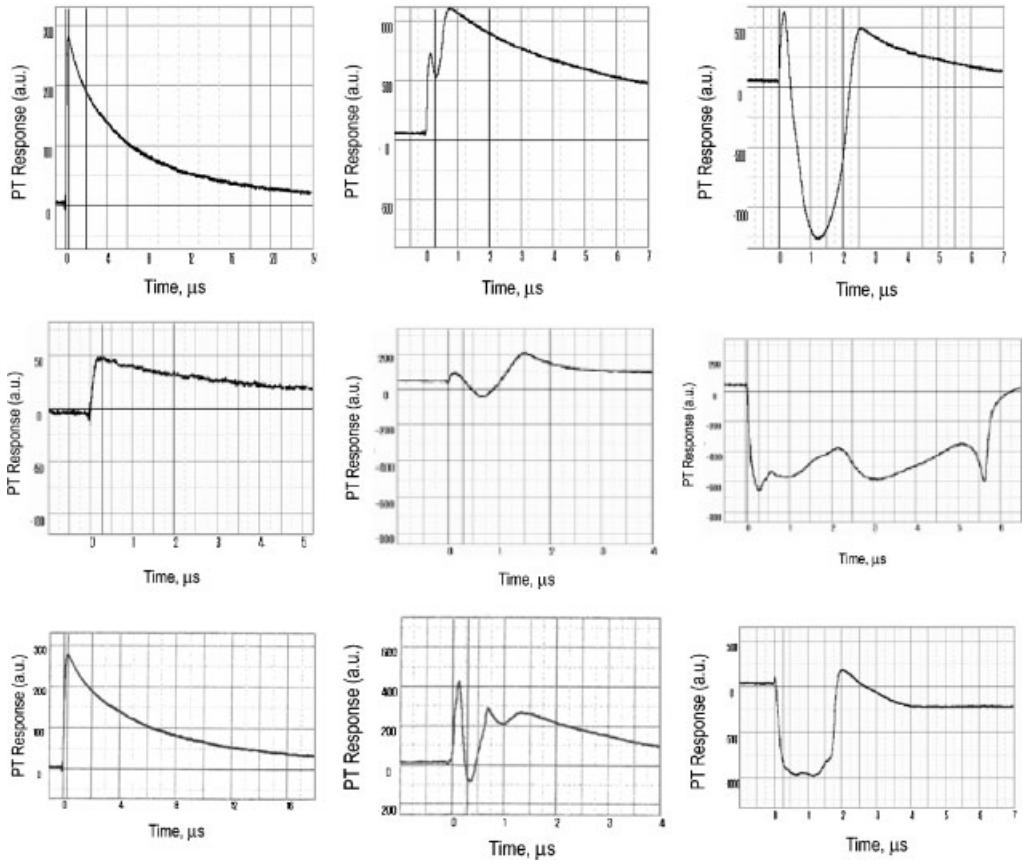

Fig. 4. Temporal shape of integrated PT responses in linear mode (type 1 responses) (left) and non-linear mode (type 2) (middle and right). Cells/wavelength/energy level (from left to right): First row, RBCs/532 nm/ 1 μJ, 4.3 μJ, and 8 μJ; second row, lymphocytes/427 nm/50 μJ, 100 μJ, and 150 μJ; third row, K562 cells/427 nm/50 μJ, 100 μJ, and 150 μJ.

levels. A similar effect was observed for all cells: an almost linear relationship between PT response and laser energy level at low energy levels (with temporal-shape response shown in Fig. 4, left), and then a saturation effect and a decay in the response amplitude. At these energy levels, dependence of the peak PT signal on the pump-pulse energy level was saturated (not shown) and led to formation of a negative peak (Fig. 4, middle and right columns), compared with a "positive" change in refraction in water-containing cells (Fig. 4, left). Indeed, in linear mode, the temperature-dependent changes in the refractive index (Δn) can be estimated as follows: $\Delta n = (dn/dT)\Delta T$, where ΔT is the laser-induced temperature elevation and dn/dT is the temperature-dependent refractive gradient (for water, -0.8×10^{-4} $[^\circ C]^{-1}$) [16,24]. Therefore, for a typical temperature range $\Delta T = 10–150^\circ C$ (the maximum is close to the bubble-formation threshold), $\Delta n = 10^{-3}–10^{-2}$, whereas the appearance of bubbles created a more significant (at least one order of magnitude higher) refractive gradient, $\Delta n = 0.33$ [25,26]. The sign of PT responses ("positive" or "negative") depends also on spatial shape of laser-induced refractive heterogeneities (e.g., this shape is close to plate-like in case cells on substrate at linear effect and close to sphere in case microbubble formation).

The appearance of a negative component indicated bubble formation led to cell damage and such signals type 2) were counted for calculation of parameter PR2. In general, the negative-peak shape of the non-linear PT response was not quite reproducible from all these cells. In particular, a cell yielded a type 1 PT response with the first pulse, but it might yield a type 2 PT response after several pulses at the same energy level. This might mean that a laser energy level below the threshold value had a cumulative effect on cells and that only the first laser pulse should be analyzed to obtain accurate information on initial cell photodamage. Sometimes, the peak amplitude of the type 2 signal did not disappear after the first pulse but decreased with subsequent pulses, finally approaching to the shape of a type 1 signal.

Photodamage Phenomena

The probability of cell damage (through parameter PR2) was studied as a function of laser fluence (Fig. 5). In the case of RBC damage probability gradually increases with

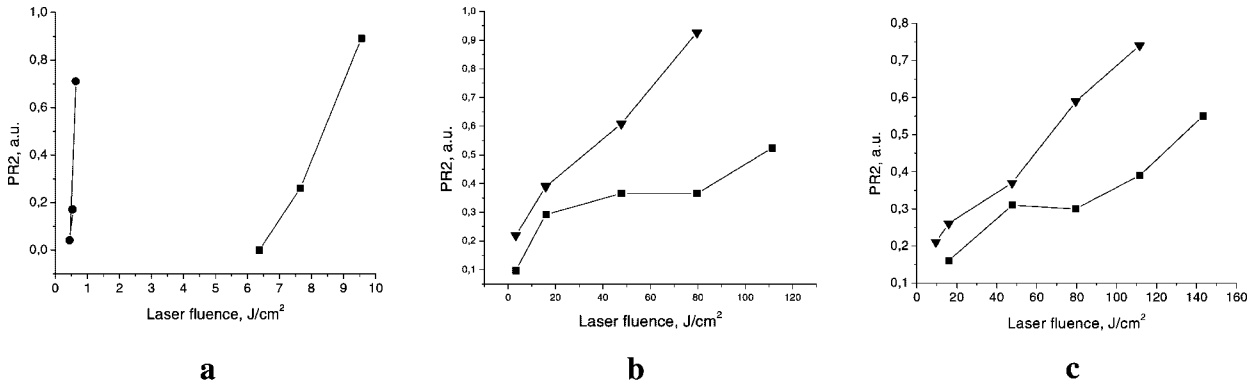

Fig. 5. Dependencies of cell damage probability PR 2 upon pump pulse fluence for RBC (**a**) ● 540 nm, ■ 434 nm, lymphocytes; (**b**) ▼ 555 nm, ■ 480 nm K562 cells; (**c**) ▼ 480 nm, ■ 555 nm as obtained at various pump laser wavelengths.

increase of laser fluence. The transition parameter PR2 from 0 to 1 to value occurs in the fluence range from 3.0 to 5.5 J/cm^2 at 532 nm. This phenomenon shows natural spread of damage thresholds among formally equal cells due to the heterogeneity of their light absorption properties. Such heterogeneity cannot be detected when cells are analyzed as whole suspension with population-averaged data being only available. White blood cells (lymphocytes and K562) revealed similar behavior. Although the fluence range that corresponded to transition of PR2 value from 0 to 1 turned out to be much wider in comparison with RBC: for lymphocytes it was 6.0 J/cm^2 and 4.7 J/cm^2 (417 nm) and for K562 it was 36 J/cm^2 (420 nm). As can be seen from Fig. 5 the damage fluencies for different white blood cells may vary by a factor of 2–3. The parameters PR2(E) were obtained at several pump wavelength: 417, 420, 427,434, 460,480, 532, 540, and 555 nm. The shape of those curves was similar for different wavelength. Damage thresholds that corresponded to 0.5 probability of cell damage for a given cell population were defined from dependence of parameter PR2(E) on laser energy. Those thresholds as obtained with LLT method were found to be 0.5 J/cm^2 and 2.3 J/cm^2 for 427 and 532 nm, respectively, for RBCs; 4.4 J/cm^2 and 42 J/cm^2 at wavelengths of 420 nm and 555 nm, respectively, for lymphocytes; and 36 J/cm^2 and 90 J/cm^2 at 420 nm and 555 nm wavelengths for tumor cells K562. This way we composed threshold spectra for each type of cells (Figs. 6 and 7). For the same sample we have obtained standard absorption spectra of cell suspensions using conventional spectrophotometer. Those spectra are given in Figures 6 and 7 also.

Regardless of the energy level, the cell viability tests consistently showed a slightly greater proportion of damaged cells (on average, 10%–20%) than were detected with PT technique. There are several possible explanations of this discrepancy. First, PT technique was not sensitive enough to detect all phenomena that led to cell damage. Besides cell damage may occur due to several processes including bubble formation and high local temperature gradient (up to 150–200°C) around absorbing zones.

Regarding RBCs, we found that the damage threshold (ED_{50}) spectrum was inversely correlated with the known absorption spectrum of the cells (Fig. 6a). For example, the ratios of the percentage of absorbed energy to the cell damage-producing laser energy level at specific wavelengths were 61%/1.84 μJ at 417 nm, 59%/2.0 μJ at 427 nm, 9.5%/26 μJ at 540 nm, and 9.92%/19 μJ at 555 nm. In particular, the ED_{50} values for RBCs at 420-nm and 532-nm wavelengths were 0.6 J/cm^2 and 5 J/cm^2, respectively. The average damage thresholds for low-absorbing lymphocytes (compared with strongly absorbing RBCs) were 4.4 J/cm^2 and 42 J/cm^2 at wavelengths of 420 nm and 555 nm, respectively. The average ED_{50} values for K562 cells, which were higher than those for lymphocytes, were 36 J/cm^2 and 90 J/cm^2 at 420-nm and 555-nm wavelengths, respectively. For white blood cells we have found the damage threshold spectra does not correlate well with absorption spectra in blue spectral range (420–460 nm). Despite increase of extinction coefficient at laser wavelengths, there was increase of threshold levels. This fact can be explained probably by false absorption curve in this wavelength range caused by scattering effects. This effect was observed for cell samples that had equal cell source to those with good correlation of threshold and absorption spectra.

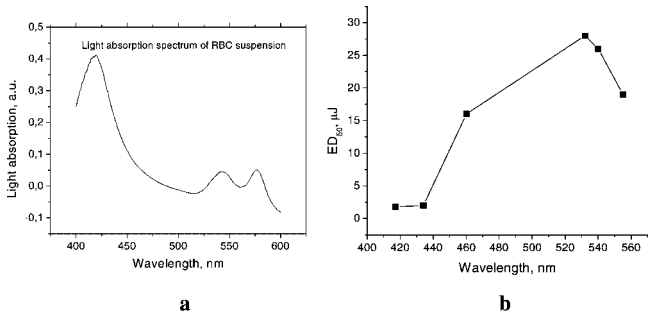

Fig. 6. Spectra: Light absorption (**a**) and photodamage threshold (ED_{50}) (**b**) for RBCs.

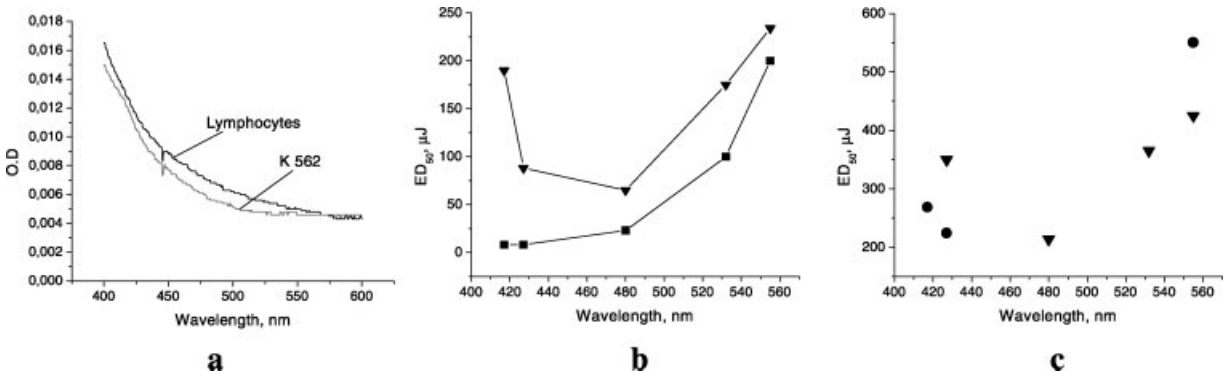

Fig. 7. Spectra: Light absorption (**a**) and photodamage threshold (ED_{50}) for lymphocytes (**b**), and K562 (**c**). Different marks indicate different cell populations with altered damage spectra.

DISCUSSION

With increased laser energy and a transition to invasive mode, strong short-term laser-induced local overheating led to cell damage. These effects were manifested as bright-light spots in the PT images (Fig. 3, right) or as a negative component in the integrated PT response (Fig. 4, middle, right). As can be seen from the corresponding PT images of all cell types, the cell damage has local nature likely due to overheating effects around the most strongly absorbing zone. Time-resolved PT monitoring of damage dynamics showed that multiple absorbing zones may be involved. The transition from 0 to 1 PR2 values occurred at a relatively broad range of pump-pulse energy levels, depending on cell type, and heterogeneity of absorbing structures. This may be caused by difference in properties of local absorbing zones (not visible by other techniques). Hence, the amplitude of both positive and negative peaks of PT signals yields information, in different ways, on local cellular absorption. In other words, laser-induced cell damage, and especially parameter PR2 is useful because (1) it provides additional information on local intracellular absorption levels and (2) it increases the sensitivity of PT detection of local absorption by at least one order of magnitude (as the maximum amplitude of the negative peak was at least one order of magnitude higher than the "positive" PT response).

The ED_{50} value for a single 8-nanosecond laser pulse in the pump wavelength range of 417–555 nm varied as follows: for RBCs, 0.5–5 J/cm^2; for lymphocytes, 4.4–42 J/cm^2; and for K562 cells, 36–90 J/cm^2. These very broad threshold parameters, especially for "non-pigmented" cells (i.e., lymphocytes and K562 cells), can be explained by (1) the presence of a different cell population, with at least two subpopulations of lymphocytes, (2) different functional states of the cells, and (3) spatially and dynamically heterogeneous absorbing microstructures. These features make it difficult to establish one damage threshold for an entire cell population. The differences in threshold levels may also be correlated with differences in the size (volume) or heat capacity of individual cells; the bigger the cell, the higher the energy density required to induce cell damage (valid at least for K562 cells). A cell's shape may also influence its damage threshold. A full understanding of the damage process, however, requires additional work. It was confirmed earlier by us [24,26] that bubble formation induced cell death without significant delay after cell irradiation. In this study, the energy was deposited in a much shorter time than the thermal relaxation time. It was clear that sudden physical (thermal) expansion was accompanied by mechanical stress. This phenomenon may influence the properties of surrounding tissues, including subcellular organelles, in different ways, such as protein and enzyme dysfunction, probable disruption of transport channels, with a damaged-area radius greater than the size of the absorbers, even if the absorber has nanoscale dimensions. Time-resolved monitoring of laser-induced cell damage clearly confirmed that for both pigmented and non-pigmented cells the damage processes can be detected and evaluated in similar way. Comparisons of damage thresholds for strongly absorbent cells, such as RBCs (0.5–1 J/cm^2 at a 420-nm wavelength with a hemoglobin absorption coefficient of around 1,100–1,300 cm^{-1} [23]), with data obtained with pigmented retinal cells (0.1–0.8 J/cm^2 at 694 nm and 532 nm wavelengths, with a melanin absorption coefficient of around 1,000–1,900 cm^{-1} [2,5,7]) show similar threshold parameters. There are no available data for comparisons with other non-pigmented cells. In general, however, laser-induced cell damage likely has a main mechanism that is non-specific to cells type and is the result of local absorption, probably by several mixed types of absorbing chromophores, with corresponding overheating of the most strongly absorbing local zones. This assumption can also be proved by correlation of light absorption spectra and damage threshold spectra of studied cells. It should be noted that in terms of light absorption RBC and K562 cells are totally different—former have uniform light absorption and latter have localized absorption structure. Nevertheless the both types of cells yielded similar correlation of their damage threshold spectra with absorption spectra.

CONCLUSION

We have demonstrated that PT method can be used in two modes and it is a very useful tool with diagnostic value for: (a) the imaging of intracellular chromophores distributed in living single cells; (b) visualization of laser-induced local thermal effects; and (c) for time-resolved monitoring of cellular damage, which is likely associated in many cases with bubble formation phenomena. PT analysis of a cell population (100–150 cells) can be completed within 10 minutes (PT-response mode) to 20 minutes (imaging mode). This method has the potential to obtain information on non-fluorescent local absorbing structures of average size that may be below the diffraction limit [24,25,29]. A great advantage of the PT imaging technique is that laser scanning is not required, as the whole cell is simultaneously irradiated with broad-diameter pump and probe beams and spatial resolution is determined by the microscopic scheme used. This solution also avoids the need for precise cell positioning. In principle, after additional calibration, this new technique will allow estimating laser-induced local temperature, which is important for optimizing laser cellular micro- or even nano-surgery. The exact mechanisms of laser-induced damage, as well as the nature of absorbing zones, however, are still unclear and require further study, especially in vivo. Efforts to use the PT technique to monitor damage threshold due to bubble formation in vivo are currently underway in our laboratory.

Thus, the main findings of this work are:

- Thresholds of laser-induced damage may vary significantly among individual cells; this may require redefinition of "damage threshold" criteria at tissue or organ level;
- The more complex the local absorbing structure of cells, the more will be the variation of laser damage thresholds among them;
- Damage threshold spectra in visible range as a rule are correlated (inverse proportionally) with absorption spectra for cell suspensions;
- Laser-induced damage in individual "non-pigmented" cells at nanosecond pulse duration is associated with thermally-induced phenomena (e.g. bubble formation effects), that is in line with data by another researchers [13,15,19,21] for pigmented cells.

ACKNOWLEDGMENTS

The work described was performed at the University of Arkansas for Medical Sciences (UAMS) during visit of D. Lapotko, PhD in UAMS and supported by grants to VPZ from the National Science Foundation (BES0119470). The authors thank M. Cannon, PhD, of the Department Microbiology and Toxicology at UAMS for his significant help with cell sample preparation in his laboratory and consultation regarding cell properties, V. Galitovsky, PhD for estimating cell viability in selected experiments, and Scott Ferguson for his assistance with laser measurements.

REFERENCES

1. Sliney DH, Wolbarsht ML. Safety with lasers and others optical sources. New York: Plenum Publishing 1980.
2. Rounds DE. Effect of laser radiation on cell culture. Fed Proc 1965;24S:116–121.
3. Rounds DE. Laser radiation of tissue cultures. Ann N Y Acad Sci 1965;122:713–720.
4. Bersns MW, Rounds DE, Olson RS. Effects of laser microirradiation on chromosomes. Exp Cell Res 1969;56:292–298.
5. Beilin E, Buyanov-Uzdalsky AY, Lotchilov VI, Zharov VP. Investigation of laser-induced acoustic effects in water and their influence on cell structure. Acoust Phys 1987;33:344–349.
6. Zharov VP, Kilpio AV, Lotchilov VI, Shashkov VB. Application of power optoacoustic methods and instruments in medicine and biology. In: Hess P, Pelzl J, editors. Photoacoustics and photothermal phenomena. Berlin, New York: Springer-Verlag 1987:533–547.
7. Berns MW, Floyed AD, Olnuki Y. Chromosome lesions produced with an argon laser microbeam without dye sensitization. Science 1971;171:903–905.
8. Ara G, Anderson RR, Mandel KG, Ottesen M, Oseroff AR. Irradiation of pigmented melanoma cells with high intensity pulsed radiation generates acoustic waves and kills cells. Lasers Surg Med 1990;10:52–59.
9. Vogel A, Schweiger P, Frieser A, Asiyo MN, Birngruber R. Intraocular Nd:YAG laser surgery: Laser-tissue interaction, damage range, and reduction of collateral effects. IEEE J Quant Electron 1990;20:2240–2260.
10. Jacques SL, McAuliffe DJ. The melanosome: Threshold temperature for explosive vaporization and internal absorption coefficient during pulsed laser irradiation. Photochem Photobiol 1991;53:769–775.
11. Doukas AG, McAuliffe DJ, Flotte TJ. Biological effects of laser-induced shock waves: Structural and functional cell damage in vitro. Ultrasound Med Biol 1993;19:137–146.
12. Roider J, Hillenkamp F, Flotte T, Birngruber R. Microphotocoagulation: Selective effects of repetitive short laser pulses. Proc Natl Acad Sci USA 1993;90:8643–8647.
13. Doukas AG, McAuliffe DJ, Lee S, Venugopalan V, Flotte TJ. Physical factors involved in stress-wave-induced cell injury: The effect of stress gradient. Ultrasound Med Biol 1995;21:961–967.
14. Doukas AG, Flotte TJ. Physical characteristics and biological effects of laser-induced stress waves. Ultrasound Med Biol 1996;22:151–164.
15. Lee S, Anderson T, Zhang H, Flotte TJ, Doukas AG. Alteration of cell membrane by stress waves in vitro. Ultrasound Med Biol 1996;22:1285–1293.
16. Gerstman BS, Thompson CR, Jacques SL, Rogers ME. Laser-induced bubble formation in the retina. Lasers Surg Med 1996;18:10–21.
17. Lee S, McAuliffe DJ, Zhang H, Taitelbaum J, Xu Z, Flotte TJ, Doukas AG. Stress-wave-induced membrane permeation of red blood cells is facilitated by aquaporins. Ultrasound Med Biol 1997;23:1089–1094.
18. Lin CP, Kelly MW. Cavitation and acoustic emission around laser-heated microparticles. Appl Phys Lett 1998;72:2800–2802.
19. Jay DG. Selective destruction of protein function by chromophore-assisted laser inactivation. Proc Natl Acad Sci USA 1988;85:5454–5458.
20. Huttmann G, Birngruber R. On the possibility of high-precision photothermal microeffects and the measurement of fast thermal denaturation of proteins. IEEE J Sel Topics Quant Electron 1999;5:954–962.
21. Lin CP, Kelly MW, Sibayan SA, Latina MA, Anderson RR. Selective cell killing by microparticle absorption of pulsed laser radiation. IEEE J Sel Topics Quant Electron 1999;5:963–968.
22. Leszczynski D, Pitsillides CM, Pastila RK, Rox Anderson R, Lin CP. Laser-beam-triggered microcavitation: A novel method for selective cell destruction. Radiat Res 2001;156:399–407.

23. Welch AJ, van Gemert MJ, editors. Optical-thermal response of laser-irradiated tissue. New York: Plenum Publishing 1995.
24. Lapotko DO, Romanovskaya TR, Shnip A, Zharov VP. Photothermal time-resolved imaging of living cells. Lasers Surg Med 2002;31:53–63.
25. Zharov VP, Galitovsky V., Viegas M. Photothermal detection of local thermal effects during selective nanophotothermolysis. Appl Phys Letter 2003;83(24):4897–4899.
26. Lapotko DO, Lukianova EY, Ship AI. Photothermal detection of laser-induced damage in single intact cells. Lasers Surg Med 2003;33:320–329.
27. Lapotko D, Kuchinsky G, Potapnev M, Pechkovsky D. Photothermal image cytometry of human neutrophils. Cytometry 1996;24:198–203.
28. Lapotko D, Romanovskaya T, Zharov V. Photothermal images of live cells in presence of drug. J Biomed Opt 2002; 7:425–434.
29. Zharov V, Lapotko D. Photothermal sensing of nanoscale targets. Rev Sci Instrum 2003;74:785–788.